**H1prelim-09-017** Submitted to

**XVII International Workshop on Deep Inelastic Scattering, DIS2009**, April 26-30, 2009, Madrid
Parallel Session **Diffraction and vector mesons**

*Electronic Access: www-h1.desy.de/publications/H1preliminary.short_list.html*

# Diffractive electroproduction of $\rho$ and $\phi$ mesons at HERA

H1 Collaboration

**Abstract**

This preliminary result reports on the H1 analysis of HERA-1 data for $\rho$ and $\phi$ VM diffractive production, both in the elastic and proton dissociative channel. Plots presented here are complementary to the previous preliminary report (H1prelim-08-013) to be found at www-h1.desy.de/publications/H1preliminary.short_list.html.

# References


[1] A. Aktas *et al.* [H1 Collaboration], Eur. Phys. J. **C46** (2006) 585 [hep-ex/0510016].

[2] J. Breitweg *et al.* [ZEUS Collaboration], Eur. Phys. J. **C14** (2000) 213 [hep-ex/9910038];

[3] S. Chekanov *et al.* [ZEUS Collaboration], PMC Phys. **A1** (2007) 6 [hep-ex/0708.1478].

[4] S. Chekanov *et al.* [ZEUS Collaboration], Nucl. Phys. **B 718** (2005) 3 [hep-ex/0504010].

[5] S. Chekanov *et al.* [ZEUS Collaboration], Eur. Phys. J. **C24** (2002) 345 [hep-ex/0201043].

[6] S. Chekanov *et al.* [ZEUS Collaboration], Nucl. Phys. **B 695** (2004) 3 [hep-ex/0404008].

[7] S. Aid *et al.* [H1 Collaboration], Nucl. Phys. **B468** (1996) 3 [hep-ex/9602007].

[8] S.V. Goloskokov and P. Kroll, Eur. Phys. J. **C53** (2008) 367.

[9] I.P. Ivanov, N.N. Nikolaev and A.A. Savin, Phys. Part.Nucl. 37 (2006) 1.

[10] A.D. Martin, M.G. Ryskin and T. Teubner, Phys. Rev. **D55** (1997) 4329.

[11] H. Kowalski, L. Motyka and G. Watt, Phys. Rev. **D74** (2006) 074016.

[12] P. Amaudruz *et al.* [NMC Collaboration], Z. Phys **C54** (1992) 239;
M. Arneodo *et al.* [NMC Collaboration], Nucl. Phys. **B429** (1994) 503.

[13] M.R. Adams *et al.* [E665 Collaboration], Z. Phys **C74** (1997) 237.

[14] A. Airapetian *et al.* [HERMES Collaboration], Eur. Phys. J. **C 17** (2000) 389; K. Ackerstaff *et al.* [HERMES Collaboration], Eur. Phys. J. **C 18** (2000) 303;
A. Airapetian *et al.* [HERMES Collaboration], Eur. Phys. J. **C ??** (??) ??.

[15] K.J. Golec-Biernat and M. Wüsthoff, Phys. Rev. **D59** (1999) 014017;
*idem*, Phys. Rev. **D60** (1999) 114023.

[16] J. Pumplin *et al.* [CTEQ Collaboration], JHEP 0207 (2002) 012, [hep-ph/0201195]; *idem*, JHEP 0702 (2002) 053, [hep-ph/0611254].

[17] C. Marquet, R. Peschanski and G. Soyez, Phys. Rev. **D76** (2007) 034011.

[18] T. Teubner, private communication.

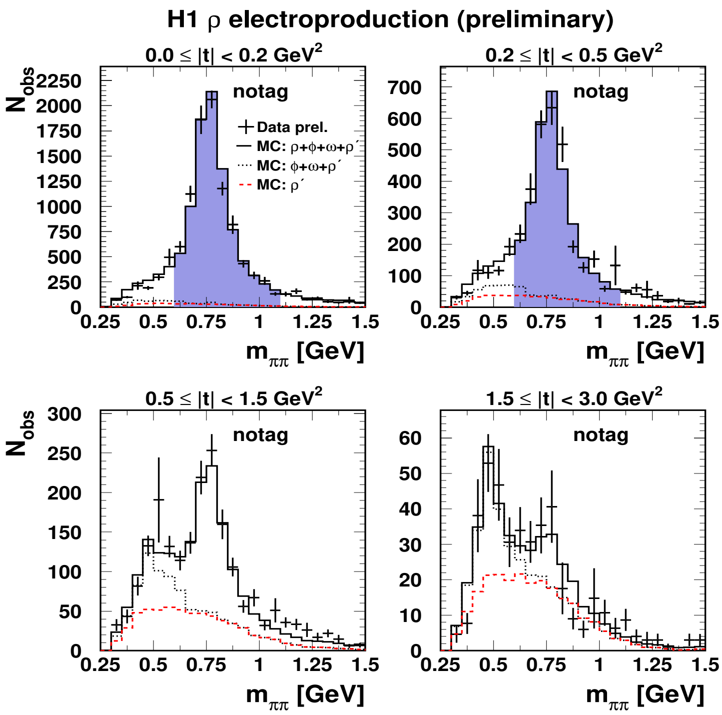


Figure 1: Distributions of the $m_{\pi\pi}$ invariant mass (with the cut $m_{KK} > 1.04\ \mathrm{GeV/c^2}$ to reject the $\phi \rightarrow KK$ signal) in four domains in $|t|$, for the notag sample. The dashed histograms show the MC predictions for the $\rho'$ background, the dotted histograms the sum of the $\rho'$, $\omega$ and $\phi$ backgrounds, and the full histograms the $\rho$ signal (including interference with $\pi\pi$ non-resonant production) and the sum of all backgrounds. The mass and $|t|$ domain where the cross section measurements are performed is shaded.

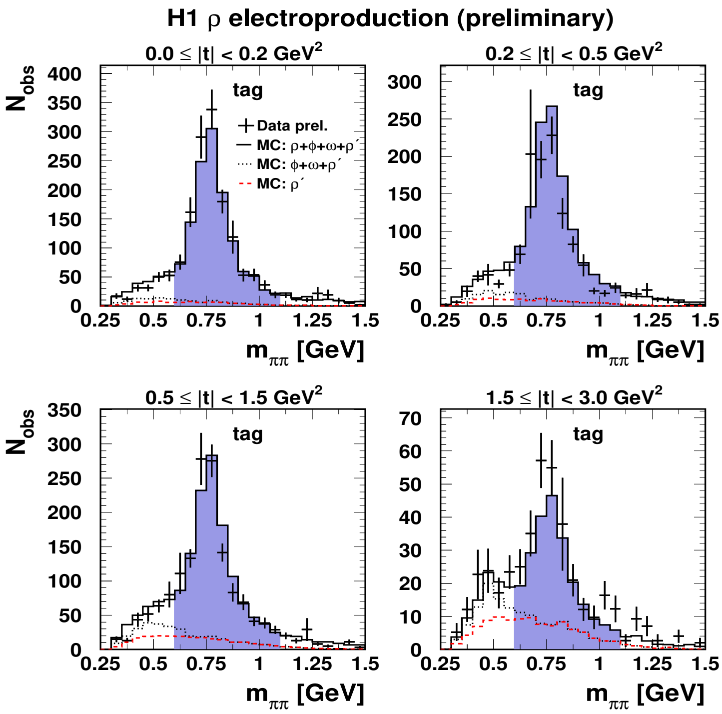


Figure 2: Same as in Fig. 1, for the tag sample.

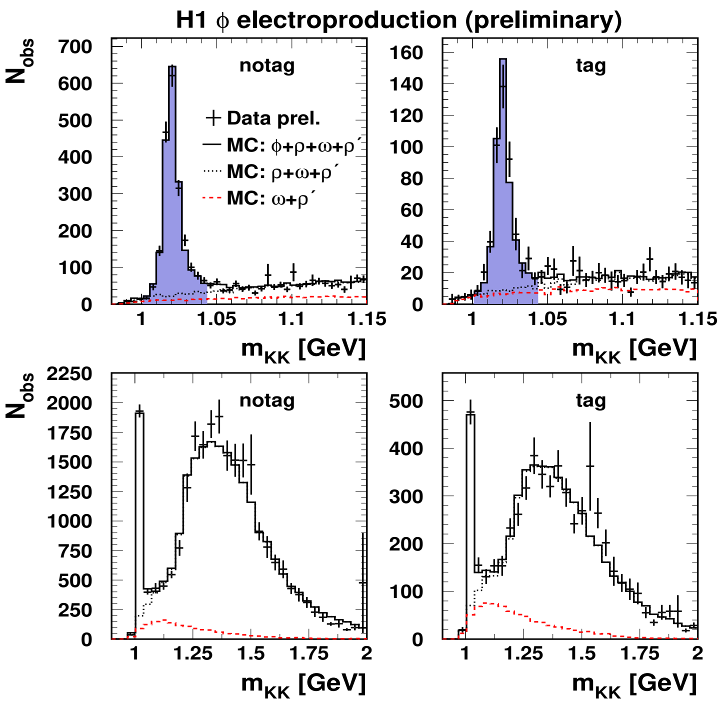


Figure 3: Distributions of the $m_{KK}$ invariant mass: (a)-(b) in the $\phi$ mass region (notag and tag samples, respectively); (c)-(d) over an extended mass range, showing the $\phi$ signal and the $m_{KK}$ reflection of $\rho$ and background productions. The dashed histograms show the sum of the $\rho'$, $\omega$ and $\phi \to\ 3\,\pi$ backgrounds, the dotted histograms show in addition the $\rho$ and non-resonant $\pi\pi$ backgrounds, and the full histograms the $\phi \to\ KK$ signal and the sum of all backgrounds. In (a) and (b), the mass domain where the cross section measurements are performed is shaded.

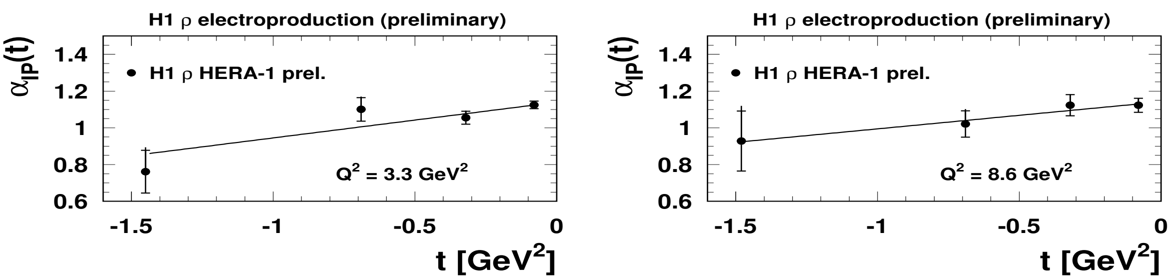


Figure 4: $t$ dependence of the values of the $\alpha_{I\!P}(t) = \delta(t)/4 + 1$ parameters obtained from the linear fits to the $W$ dependences. for (a) $Q^2 = 3.3\ \mathrm{GeV}^2$; (b) $Q^2 = 8.6\ \mathrm{GeV}^2$. The lines are the results of linear fits of the form of $\alpha_{I\!P}(t) = \alpha_{I\!P}(0) + \alpha'\,t$

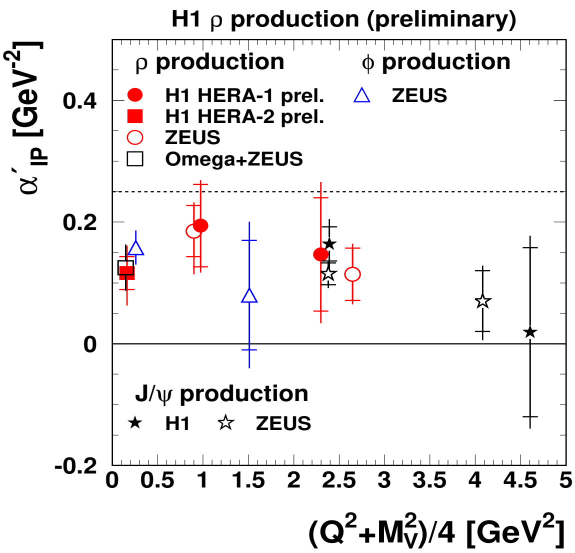


Figure 5: Measurements by H1 [1] and ZEUS [2–6] of the slope of the effective pomeron trajectory $\alpha'$ for VM photo- and electroproduction.

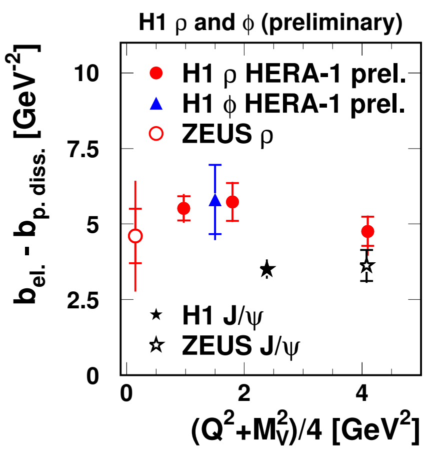


Figure 6: Slope differences $b_{el.} - b_{p.\ diss.}$ between elastic and proton dissociative scattering for $\rho$ and $\phi$ meson production, as a function of $(Q^2 + M_V^2)/4$. Results of ZEUS $\rho$ photoproduction [2] and of H1 [1] and ZEUS [5,6] $J/\psi$ photo- and electroproduction are also shown.

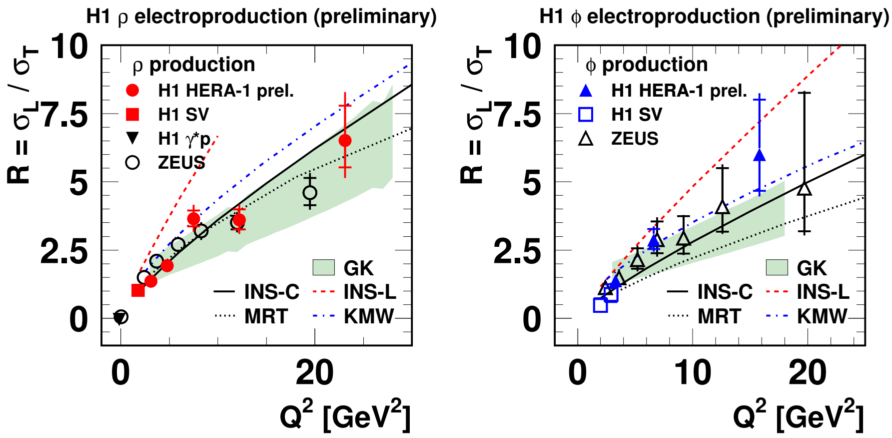


Figure 7: $Q^2$ dependence of the ratio $R = \sigma_L$ / $\sigma_T$ of the longitudinal to the transverse cross sections for (a) $\rho$ meson production; (b) $\phi$ production. Measurements of $R$ in the SCHC approximation, for $\rho$ photoproduction by H1 [7] and ZEUS [2] and for $\rho$ and $\phi$ electroproduction by ZEUS [2–4] are also shown. The superimposed curves are predictions of the models of GK [8], INS [9] with "compact" (INS-C) and "large" (INS-L) WF's, MRT with the CTEQ6.5M PDF parameterisation [10] and KMW [11].

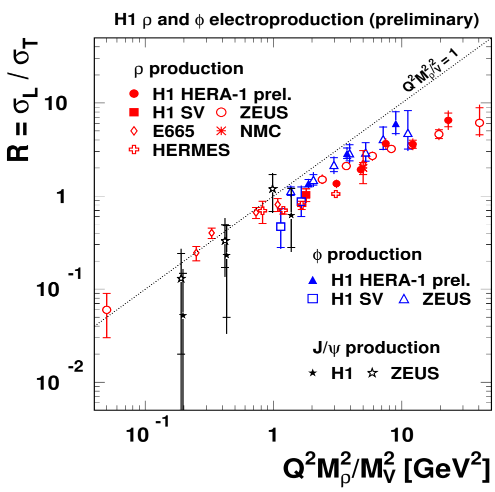


Figure 8: Ratio $R = \sigma_L$ / $\sigma_T$ as a function of the variable $Q^2 \cdot M_\rho^2$ $/M_V^2$. Electroproduction measurements of $\rho$ mesons by fixed target experiments (NMC [12], E665 [13] and HERMES [14]), of $\rho$ and $\phi$ mesons by ZEUS [3, 4] and of $J/\psi$ mesons by H1 and ZEUS [1, 6] are also shown. The dotted line represents the scaling behaviour $R = Q^2 \cdot M_\rho^2$ $/M_V^2$.

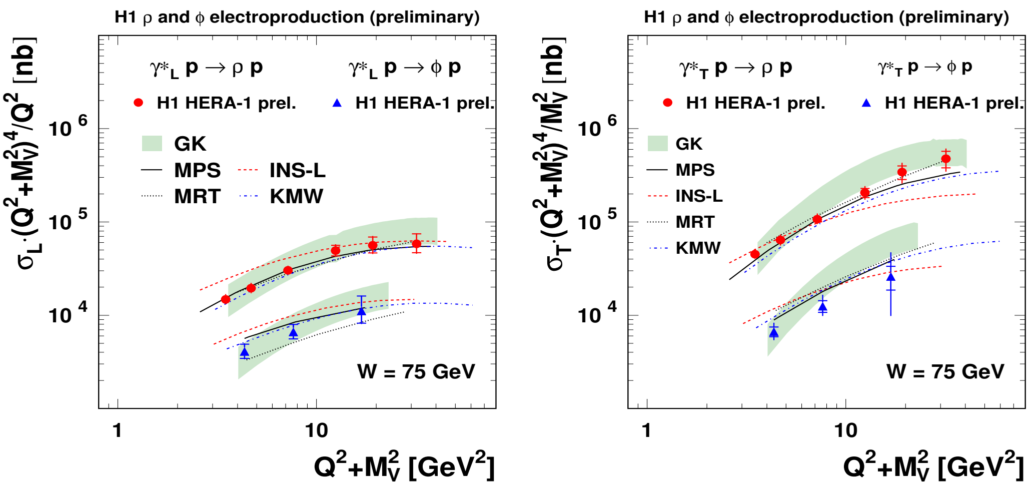


Figure 9: $(Q^2+M_V^2)$ dependences of VM $\gamma^* p$ cross sections for for $\rho$ and $\phi$ elastic production with $W = 75$ GeV: (a) longitudinal cross sections, multiplied by the scaling factor $(Q^2 + M_V^2)^4/Q^2$; (b) transverse cross sections, multiplied by $(Q^2 + M_V^2)^4/M_V^2$. The superimposed curves are predictions of the models of GK [8], KMW [11] with GW saturation [15], MRT [10] with the CTEQ6.5M PDF's [16], INS [9] (compact WF) and MPS [17].

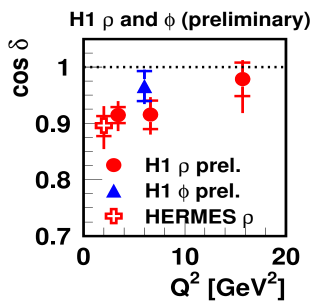


Figure 10: Cosine of the phase $\delta$ between the $T_{00}$ and $T_{11}$ helicity conserving amplitudes for $\rho$ and $\phi$ production with $|t| \le 0.5$ GeV$^2$, measured as a function of $Q^2$ in the SCHC approximation. The HERMES [14] measurement on protons is also shown. The dotted line indicates the value 1 which corresponds to amplitudes in phase.

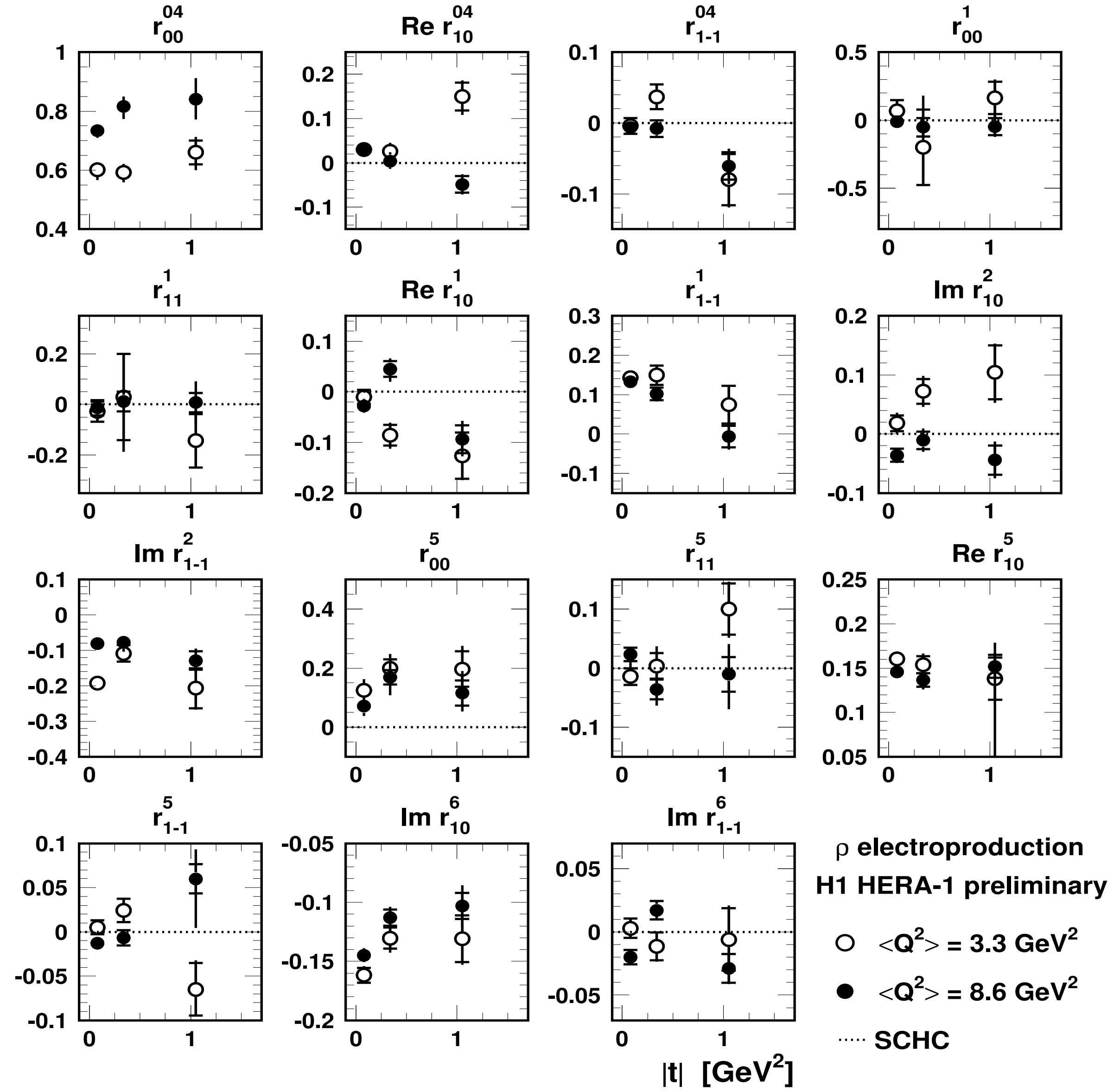


Figure 11: Spin density matrix elements for the diffractive electroproduction of $\rho$ mesons, as a function of $|t|$, for two intervals in $Q^2$: $2.5 \leq Q^2 < 5\ \mathrm{GeV}^2$ and $5 \leq Q^2 \leq 60\ \mathrm{GeV}^2$.

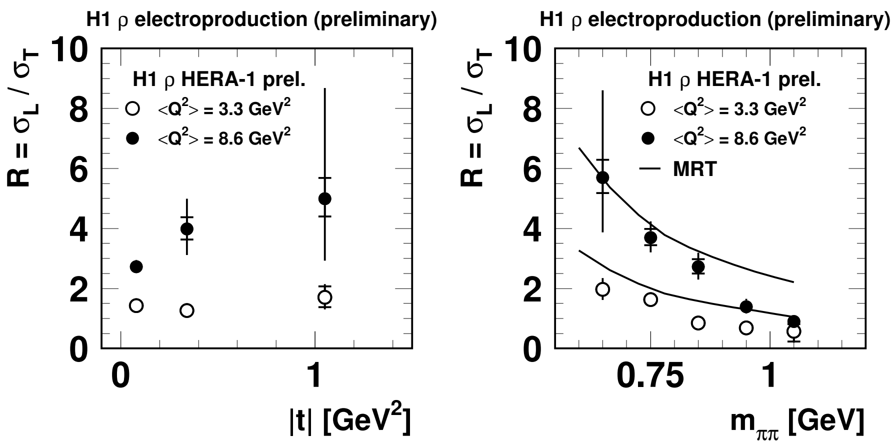


Figure 12: Dependence, for $\rho$ meson production, of the ratio $R = \sigma_L$ / $\sigma_T$ of the longitudinal to the transverse cross sections, on (a) $|t|$; (b) $m_{\pi\pi}$, separately for $2.5 \leq Q^2 < 5$ GeV$^2$ and for $5 \leq Q^2 \leq 60$ GeV$^2$. The curves in (b) are from the MRT model [18].

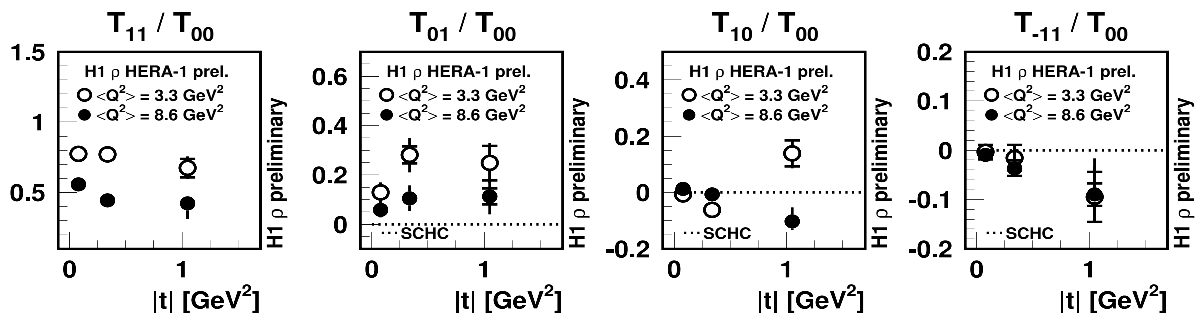


Figure 13: Ratios of the helicity amplitudes, computed from global fits to the measurements of the 15 spin density matrix elements, as a function of $|t|$ for $\rho$ meson production and for two bins in $Q^2$: $2.5 \leq Q^2 < 5$ GeV$^2$ (open circles) and $5 \leq Q^2 \leq 60$ GeV$^2$ (closed circles). NPE is assumed and all amplitudes are taken as purely imaginary. Where appropriate, the dotted lines show the expected null value of the ratio if the non-SCHC amplitudes are vanishing.